Effects of Ag^+ Ion Doping on UV Radiation Absorption and Luminescence Profiles of Fluorapatite Nanomaterials Obtained by Neutralization Method

D.V. Milojkov[a,b,*], V.Dj. Stanić[b], S.D. Dimović[b], D.R. Mutavdžić[c], V. Živković-Radovanović[d], G.V. Janjić[e] and K. Radotić[c]

[a]Faculty of Technology Novi Sad, University of Novi Sad, Bulevar Cara Lazara 1, 21000 Novi Sad, Serbia
[b]Vinča Institute of Nuclear Sciences, University of Belgrade, P.O. Box 522, 11001 Belgrade, Serbia
[c]Institute for Multidisciplinary Research, University of Belgrade, Kneza Višeslava 1, 11030 Belgrade, Serbia
[d] Faculty of Chemistry, University of Belgrade, Njegoševa 12, 11001 Belgrade, Serbia
[e]Institute of Chemistry, Technology and Metallurgy, University of Belgrade, Njegoševa 12, 11001 Belgrade, Serbia

(Received June 20, 2018; revised version April 4, 2019; in final form April 16, 2019)

In the present study we have analyzed effects of Ag^+ ions doping on energetic profiles of nanophosphors materials based on fluorapatite crystal system. The UV radiation absorption and luminescence properties of monophase fluorapatite (FAP) and Ag^+ doped fluorapatite (AgFAP) nanomaterials obtained by neutralization method were investigated using the photoluminescence spectrophotometry. The excitation-emission profiles of nanomaterials were analyzed statistically by MCR-ALS method and number of fluorophores was extracted. FAP lattice absorbed light at 350 nm in the UVA part of spectrum, and with increasing concentration of Ag^+ ions new absorption maximum appeared at 270 nm in the UVC part. Fluorescence of FAP nanoparticles was in violet region of visible part of the spectrum, with a red shift to the green region when Ag^+ was doped in lattice. MCR-ALS analyses of fluorescence spectra confirm formation of two maxima, at 484 and 505 nm, as a consequence of Ag^+ ions doping in FAP lattice at Ca1 (4f) sites. The results of quantum chemical calculations showed that an Ag^+ ion is stronger bonded to the binding site 1 (−1352.6 kcal/mol) than to the binding site 2 (−1249.0 kcal/mol). Considering that AgFAP1 nanopowder absorbs photons over all part of UV radiation spectrum, this material might be used as potential radiation protective nanomaterial.

DOI: 10.12693/APhysPolA.136.86

PACS/topics: silver doped fluorapatite, UV radiation, fluorescence, DFT

1. Introduction

$Ca_{10}(PO_4)_6F_2$ (FAP) nanocrystals have been playing important role in the development of suitable luminescent materials for ionizing and non-ionizing radiation dosimetry, and protection as well [1–4]. In last few decades, UV radiation measurements and protection attracted high attention considering the harmful effects on ecosystems as a consequence of degradation of ozone layer, but also the biological effects of high energy photons of the UV radiation on eyes and skin [5, 6]. Considering that biological effects are dependent on the wavelength of the incident photons, spectrum of UV radiation is subdivided into three ranges: UVA (320–400 nm), UVB (280–320 nm) and UVC (100–280 nm) [7]. On the other hand, there are also beneficial effects of UV radiation in photomedicine for phototherapy of different diseases, for water disinfection, or for increasing production of vitamins and polyphenolic compounds in fruits [7–10]. Therefore, monitoring and measurements of UV radiation is recommended, which is a reason for the development of the different types of UV dosimeters. McKinlay and Diffey, in 1987, proposed erythemal response spectrum (ERS), i.e. spectrum of the relative sensitivity of the skin to certain wavelengths of the UV radiation, as some kind of biological dosimeter [11]. Additionally, a great attention of the researchers was to develop UV dosimetric systems based on inorganic material, as well as liquid crystal mixtures [12].

Energetic profiles of FAP crystal lattice have attracted high interest for developing nanophosphors for various application areas such as solid-state laser hosts, luminescent light tubes, bio-fluorofors, as well as radiation dosimetry [13–16]. FAP crystals have structural capacity to accept many ionic substitutions, such as rare earth or transition metal ions, for creating new luminescent centers [17]. FAP as a host material provides a crystal lattice with a hexagonal symmetry space group $P63/m$, with two different Ca structural positions for substitution (Ca1 (4f) and Ca2 (6h) sites) [17]. Luminescence of FAP doped with rare-earth cations has been widely studied due to their unique optical properties [16, 17]. In addition, there are many studies of luminescence of silver nanoparticles and clusters, but there is no report on the luminescence of nanostructured fluorapatite doped with silver ions [18, 19]. In our previous study, poorly crystallized monophase nanopowders of Ag^+ doped FAP were obtained with neutralization method and charac-

*corresponding author; e-mail: d.v.milojkov@gmail.com

terized [20]. Antibacterial studies have shown that all silver-doped fluorapatite samples exhibit biocidal effect against pathogens: *Staphylococcus aureus*, *Micrococcus luteus* and *Klebsiella pneumoniae* [20]. The result of this study indicates that Ag-doped fluorapatite nanomaterials are promising as antibacterial biomaterials in orthopedics, dentistry and in the purification of waste water [20]. Along with these good biocompatible and antibacterial properties, luminescence in visible region can be additional property for different biomedical applications.

In this work we have investigated the effects of different amounts of Ag^+ ions on UV radiation absorption and luminescence properties of synthesized fluorapatite nanopowders. Also, obtained excitation-emission profiles were statistically evaluated by multivariate curve resolution-alternating least squares (MCR-ALS) method to explore fluorophores numbers of Ag^+ doped and undoped FAP samples. In addition, using quantum-chemical calculation, the differences in photoluminescence emission are expected to reveal the differences in site occupancy of Ag^+ in FAP lattice.

2. Experimental

2.1. Synthesis of FAP and Ag^+ doped FAP nanomaterials

Syntheses of nanopowders were performed according to the neutralization method and same procedure as described in our previous paper [20]. Neutralization method consists of dissolving Ag_2O in water solution of HF and H_3PO_4, and addition dropwise to suspension of $Ca(OH)_2$. Atomic ratios of [Ag/(Ag + Ca)]×100% were 0.001, 0.01 and 1%. Suspensions obtained after titration and maturation for 16 h at 20 °C where filtrated and dried at 105 °C. Finally, products were pulverized into powder, and samples were marked as FAP, AgFAP001, AgFAP01, and AgFAP1.

2.2. Photoluminescent study of obtained nanopowders

Photoluminescence spectrophotometer Horiba Jovin Yvon Fluoromax 4 TCSPC was used to characterize optical performance of samples. The photoluminescence of the samples was measured in the wavelength range of 350–600 nm. The all spectra were obtained at room temperature with an integration time of 0.1 s and 1 nm slits for excitation and emission. For each sample a series of emission spectra were collected by excitation at different wavelengths with a 3 nm step in the range of 320–350 nm for FAP, AgFAP001, and AgFAP01, and in the range of 345–370 nm for AgFAP1 sample.

2.3. Statistics and data analysis

Excitation-emission matrix with dimension 11 × 251 formed for each sample, and was analyzed by using the MCR-ALS method. This method extracted the number of components, as well as their emission and excitation profiles. All analyses were performed using The Unscramble software package (Camo ASA).

2.4. DFT calculations

The 3D coordinates of Ca(II) binding sites 1 and 2 (BS1 and BS2) were obtained from the crystal structure of fluorapatite (Fig. 1) and used for the DFT calculation. The considered FAP fragments (BS1 and BS2) were used as the model system for quantum-chemical calculations, in which Ca^{2+} ions were replaced by Ag^+ ions. The calculations of metal binding energies were done by scheme of Sakajiri et al. [21], used to calculate metal binding energies for metal ion binding to human serum transferrin. All calculations were done by using unrestricted B3LYP method, SDD basis set for metal ions and 6-31g basis set for other atoms, in Gaussian09 program (version D.01) [22], while the basis set superposition error (BSSE) was removed by counterpoise (CP) correction [23].

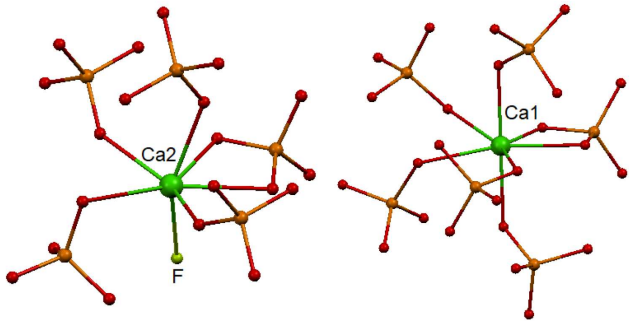

Fig. 1. Illustration of Ca2 (left) and Ca1 sites (right) in FAP crystal lattice obtained from structure in Ref. [25].

The binding energy of metal ion in binding sites 1 and 2 *in vacuo* (ΔE_M) is defined by the following formula:

$$\Delta E_M(\text{metal binding energy}) = E(\text{metal/BS complex}) - E(\text{BS}) - E(\text{free metal ion}).$$

The solvation energy of metal ion was calculated using the SMD method (at above mentioned level) with a metal ion coordinated by four water molecules in the tetrahedral geometry as a solvation model (ΔE_S) [24]. Real metal-binding energies (ΔE_R) are calculated as the difference between a metal binding energy *in vacuo* (ΔE_M) and solvation energy (ΔE_S).

3. Results and discussion

The synthesized nanoparticles were characterized by X-ray diffraction (XRD), the Fourier transform infrared (FTIR) and scanning electron microscopy (SEM) in a previous study of structural characterization of monophase FAP and AgFAP nanopowders [20]. The analysis shows that particles are of nanosize (at about an average length of 80 nm, and a width about 15 nm), and that Ag^+ ions were successfully doped in FAP crystal lattice [20]. Unit cells of apatite crystal contain two types of Ca sites, the 9-fold coordinated Ca1 sites (Wyckoff 4f position with C_3 local symmetry) and 7-fold coordinated

Ca2 sites (Wyckoff 6h position with Cs local symmetry) [25]. In the binding site 1, metal ion is surrounded by six phosphate groups, while in the binding site 2, by five phosphate groups and one fluoride anion (Fig. 1). This differences in coordination environment of the metal ions in the binding sites can be used to suggest that, on the basis of the size, Ca1 sites should be preferentially occupied by larger Ag^+ ions ($r_{Ag}^{(VII)} = 1.22$ Å) doped instead of Ca^{2+} ($r_{Ca}^{(VII)} = 1.06$ Å) [26]. Earlier research has demonstrated that monovalent larger ions such as K^+ ($r_{K}^{(VII)} = 1.46$ Å) and Na^+ ($r_{Na}^{(VII)} = 1.12$ Å) are substituted in Ca1 positions in the apatite crystal lattice, with creating a vacancy in F^- ion sites, and sometimes vacancy in Ca1 sites [27]. According to Pauling's electrostatic valency rule, local charge compensation balance is maintained with creating the empty sites [26]. This charge balance in the case of our samples is maintained by substitution of F^- ions and phosphate groups with carbonate groups, and probably with the creation of vacancies [20]. In a previous study, FTIR and chemical analyses clearly demonstrated the formation of AB-type carbonated fluorapatite structures [20].

The absorption spectra was measured for all samples at room temperature and represented in Fig. 2. Pure FAP sample have absorption maximum at about 350 nm, originated from the charge transfer (CT) transition F^- (O^{2-})–Ca^{2+} of host lattice [28, 29]. After doping of Ag^+ ions to FAP lattice, the samples still exhibited a strong broad host absorption band with little shift, and with a new absorption band which appears at 270 nm. This new absorption band might be the indication of Ag^+ substitution in Ca1 sites, and it is most probably originated from the O^{2-}–Ag^+ charge transfer transitions. With increase of dopant concentration charge transfer absorption band becomes more intensive and sharper, and proves a high efficiency of the energy transfer between the host lattice and the dopant ions. Study of optical properties of FAP microcrystals decorated with silver nanoparticles (Ag NPs) has shown that absorption of composite samples has maximum at 400 nm which can be associated with the characteristic of the surface plasmon resonance of Ag NPs [30]. These results indicate that metallic Ag NPs have formed on the surface of FAP crystals and that did not enter into the structure. Also, the diffractogram of FAP crystals decorated with Ag NPs is showing peaks originating from elemental silver, and confirm that the silver did not enter into the crystal lattice [30]. In the case of our samples, XRD diffractograms confirmed that the single phase material is obtained, which is also the proof of the Ag^+ substitution into the FAP crystal lattice [20].

Excitation-emission profiles of FAP and FAP doped with different concentration of Ag^+ ions are shown in Fig. 3.

Pure FAP sample exhibited strong broad host emission band in violet region of the visible part of spectrum. When Ag^+ ions were added to FAP lattice, the host

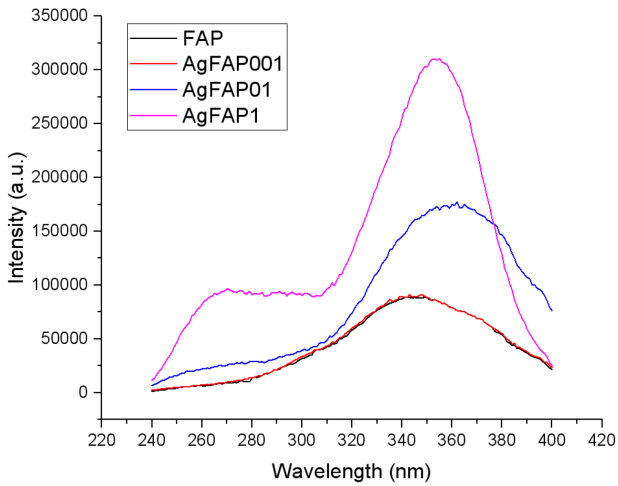

Fig. 2. Absorption spectra of FAP and FAP doped with different Ag^+ concentration.

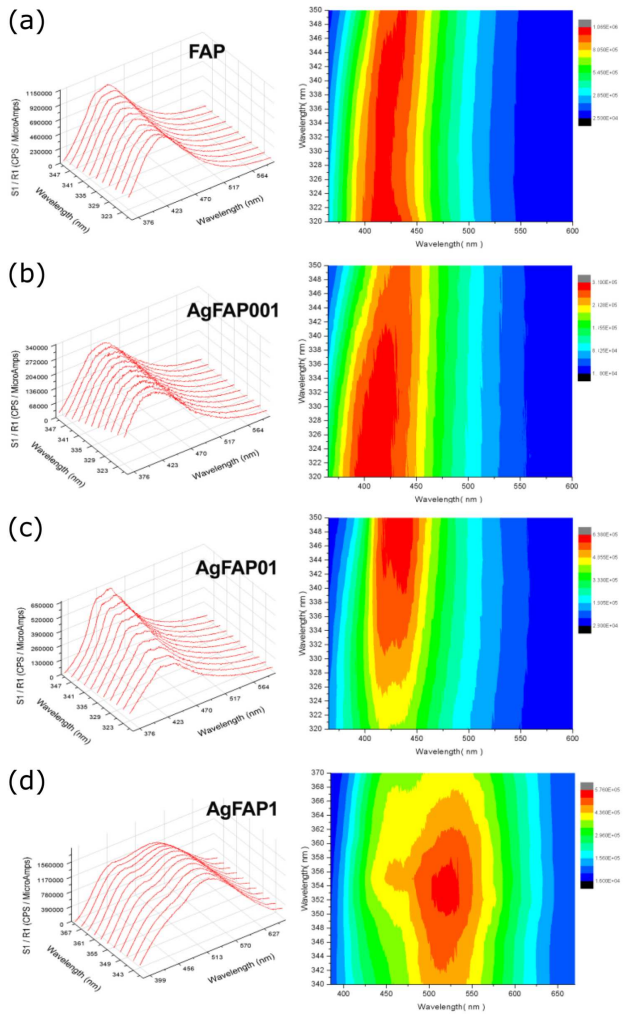

Fig. 3. Excitation-emission profiles and fluorescence contour maps of (a) FAP, (b) AgFAP001, (c) AgFAP01, and (d) AgFAP1 samples.

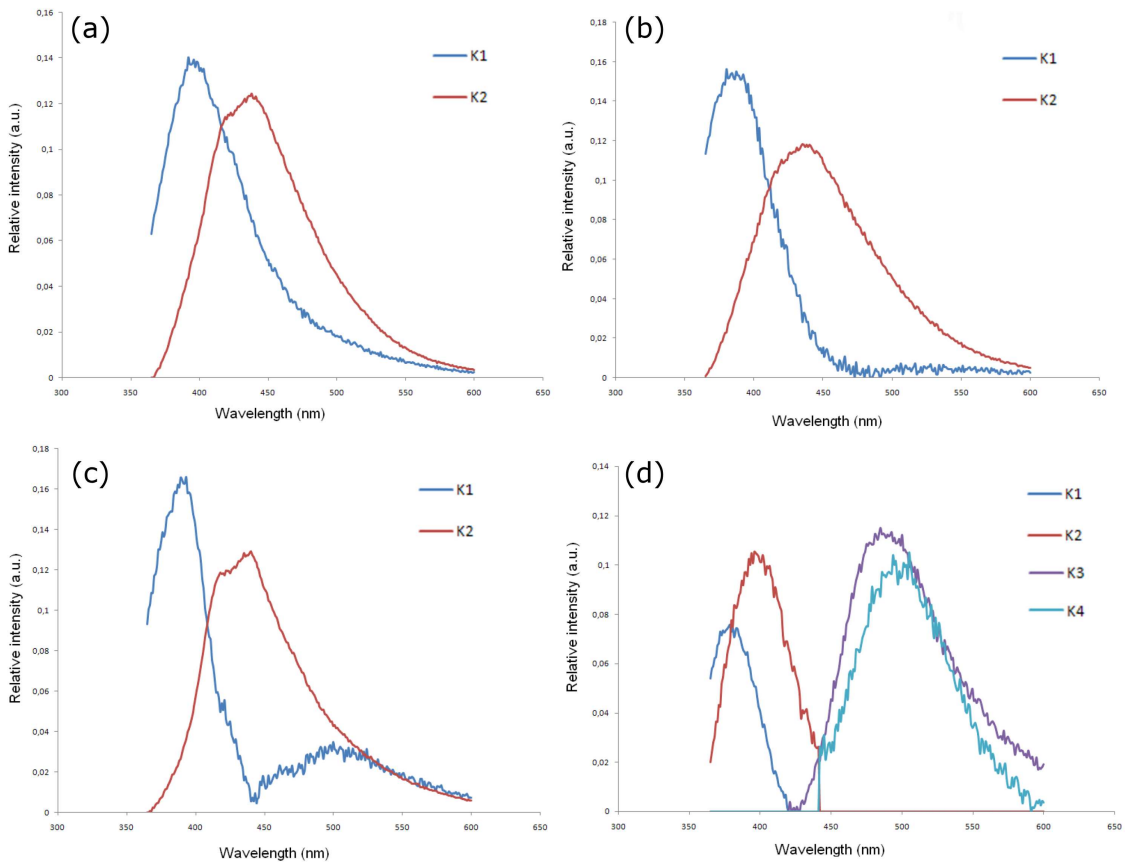

Fig. 4. Spectral components obtained using MCR-ALS analysis of excitation-emission profiles of (a) FAP, (b) AgFAP001, (c) AgFAP01, and (d) AgFAP1 samples.

emission band starting from the sample AgFAP01 displayed shoulder with the red shift in green region. Also, it can be noted an increase of emission intensity with increasing concentration of Ag^+. This is due to the creation of defects in the position of Ca2 with increasing dopant concentration, as a result of the incorporation of carbonate ions to achieve the electroneutrality of the lattice. The carbonate ions are always present when the synthesis of fluorapatite is performed in the air atmosphere, as it is shown by FTIR and thermogravimetric (TG) analyses in the previous paper [20]. Since the obtained spectra were asymmetric, MCR-ALS method was used for spectral decomposition. Component analyses of the samples are shown in Fig. 4.

Two-component analysis was adequate for all samples, except for AgFAP1 sample. In the case of this sample, with increase of Ag^+ concentration emission of host lattice was quenched, and a new emission band in green spectral range appeared. This quenching can be a consequence of creation of vacancies in the structure in Ca2 sites and F^- sites, due to the increase of Ag^+ concentration in Ca1 sites. Considering that FAP emission occurs as a result of high electronegativity of F^- from Ca2 sites, it can be concluded that the new emission in green comes from Ca1 sites. Also, for the sample AgFAP01 a new pick appears in green spectral range.

The obtained values for the emission component maximums are presented in Table I. MCR-ALS analysis shows that position of a first component K1 (blue lines in Fig. 4) is the lowest for the sample AgFAP1, and red shift occurs for all other samples. Component K2 (red lines at plots in Fig. 4) also shows the lowest value for the sample AgFAP1, and red shift occurs for all other samples. Components K3 and K4 only appear in the case of AgFAP1 sample at 484 and 505 nm. Luminescence in this region of visible part of electromagnetic spectra corresponds to the luminescence of doped silver in the other crystalline systems [31, 32].

The comparison of the binding energies *in vacuo* (ΔE_M, Table II) shows that Ag^+ ion has a higher affinity to bind in binding site 1 of fluorapatite (−1417.9 kcal/mol) than in binding site 2 (−1314.3 kcal/mol), and significantly greater affinity than the binding to the aqua complex (−121.3 kcal/mol). The values of real binding energies (ΔE_R, Table II) are slightly lower than of metal binding energies *in vacuo*, because of the desolvation of Ag^+ ions, that must be taken into account during the transition of ions from solution to crystalline state. It can be seen that the real binding energy values also indicate that Ag^+ ion is showing the strongest binding towards the binding site 1 (−1352.6 kcal/mol).

TABLE I

Values of component maxima of the samples obtained with MCR-ALS analysis

Sample	Component maxima			
	K1	K2	K3	K4
FAP	392	438	–	–
AgFAP001	380	435	–	–
AgFAP01	389	447	–	–
AgFAP1	379	397	484	505

TABLE II

Binding energies (in kcal/mol) for binding Ag^+ ion in BS1 and BS2 environment of fluorapatite, and in tetraaqua complex

Model system	Metal binding energy *in vacuo* (ΔE_M)	Solvation energy (ΔE_S)	Real binding energies (ΔE_R)
Ag^+/BS1	−1417.9	−65.3	−1352.6
Ag^+/BS2	−1314.3	−65.3	−1249.0
$[Ag(H_2O)_4]^+$	−121.3	−65.3	−56.0

The higher value of ΔE_R in the case of Ag^+ ion in BS1 could be explained by stronger electrostatic interactions of Ag^+ ion with groups from the binding site 1 (6 phosphate groups — overall charge is −18) than with groups from the binding site 2 (5 phosphate groups and one F^- ion — overall charge is −16). However, the incorporation of Ag^+ ions at binding site 2 results in a decrease of the electrostatic repulsion between the metal ions, that are closer to each other (4.00 Å), than in binding site 1 (5.43 Å). Taking into account the reduction of electrostatic repulsive forces between the metal ions and the difference in the binding energy for BS1 and BS2 of about 100 kcal/mol (about 8% of the total binding energy), it can be expected that under certain conditions, the binding Ag^+ ion at binding site 2 is possible.

Considering that the absorption of obtained AgFAP1 nanomaterial occurs in the field of UVA, UVB and UVC part of the spectrum, it can be concluded that the obtained nanoparticles may be suitable for applications as absorber of UV radiation in different cosmetic, pharmaceutical, and packing products [33–36].

4. Conclusions

The luminescence properties of FAP and Ag^+ ions doped FAP nanomaterials prepared by neutralization method were investigated by photoluminescence spectral measurements, multivariate analysis of obtained spectra, and DFT calculations. FAP lattice absorbed light at 350 nm in UVA part of spectrum, and with increasing concentration of Ag^+ ions a new absorption maximum appears at 270 nm in the UVC part. The FAP lattice shows emissions in violet range of visible light, which shifts into green region with increasing Ag^+ concentration. MCR-ALS analysis of fluorescence spectra shows good separation of luminescence from Ca1 and Ca2 sites, and indicates that Ag^+ ions are incorporated in FAP lattice at Ca1 (4f) sites. The assumed substitution mechanism in FAP lattice implies creation of defects in Ca2 and F sites, because of CO_3^{2-} ions substitution. Based on quantum-chemical calculations, it is possible to conclude that Ag^+ ion has a slightly higher affinity to the binding site 1 (−1352.6 kcal/mol) than to the binding site 2 (−1249.0 kcal/mol). Absorption of AgFAP1 nanomaterials in the whole range of the UV spectrum, and their luminescence in visible light, promises the way for potential development of a photoluminescence dosimeter for UV radiation. Taking into account their improved biocompatible and antibacterial properties, such UV radiation absorbers can be added in different cosmetics and pharmaceutical preparations for skin protection, as well as in biopolymers as filers for developing active packing materials.

Acknowledgments

This work was developed within the projects No. III 43009 and OI 173017 supported by the Ministry of Education, Science and Technological Development of the Republic of Serbia. Numerical simulations were run on the PARADOX supercomputing facility at the Scientific Computing Laboratory of the Institute of Physics, Belgrade, supported in part by the Ministry of Education, Science and Technological Development of the Republic of Serbia.

References

[1] Y. Fukuda, *Radiat. Protect. Dosim.* **100**, 321 (2002).

[2] E.E. Jay, C. Paul, M. Fossati, M.J.D. Rushton, R.W. Grimes, *J. Mater. Chem. A* **3**, 1164 (2015).

[3] W. Ritter, T.D. Mark, *Nucl. Instrum. Methods Phys. Res.* **814**, 314 (1986).

[4] D.V. Milojkov, J. Savić, J. Maletaškić, V. Živković-Radovanović, G. V. Janjić, V. Stanić, *Proc. "5th Workshop: Specific Methods For Food Safety and Quality", 13th Int. Conf. on Fundamental and Applied Aspects of Physical Chemistry "Physical Chemistry 2016"*, Ed. V. Vasić, "VINČA" Institute Of Nuclear Sciences, Belgrade 2016, p. 150.

[5] J. Jankowski, A.B. Cader, *Int. J. Occup. Med. Environ. Health* **10**, 349 (1997).

[6] J.F. Lima, O.A. Serra, *Dyes Pigm.* **97**, 291 (2013).

[7] G. Petriasvili, A. Chanishvili, G. Chilaya, M.A. Matranga, M.P. De Santo, R. Barberi, *Mol. Cryst. Liq. Cryst.* **500**, 82 (2009).

[8] X. Zhou, Z. Li, J. Lan, Y. Yan, N. Zhu, *Ultrason. Sonochem.* **35**, 471 (2017).

[9] P. Carbonell-Bejerano, M.P. Diago, J. Martínez-Abaigar, J.M. Martínez-Zapater, J. Tardáguila, E. Núñez-Olivera, *BMC Plant Biol.* **14**, 183 (2014).

[10] R. Murugesan, V. Orsat, M. Lefsrud, *Food Nutrit. Sci.* **3**, 774 (2012).

[11] A.F. McKinlay, B.L. Diffey, *CIE J.* **6**, 17 (1987).

[12] P.S. Halasyamani, W. Zhang, *Inorg. Chem.* **56**, 12077 (2017).

[13] R. Mazelsky, R.C. Ohlmann, K. Steinbruegg, *J. Electrochem. Soc.* **115**, 68 (1968).

[14] R.C. Ohlmann, K.B. Steinbruegge, R. Mazelskyet, *Appl. Opt.* **7**, 905 (1968).

[15] P. Sobierajska, R. Pazik, K. Zawisza, G. Renaudin, J.-M. Nedelec, R.J. Wiglusz, *Cryst. Eng. Commun.* **18**, 3447 (2016).

[16] X. Hu, J. Zhu, X. Li, X. Zhang, Q. Meng, L. Yuan, J. Zhang, X. Fu, X. Duan, H. Chen, Y. Ao, *Biomaterials* **52**, 441 (2015).

[17] M. Gaft, R.G. Panczer, S. Shoval, C. Garapon, G. Boulon, W. Strek, *Acta Phys. Pol. A* **90**, 267 (1996).

[18] O.S. Wolfbeis, *Chem. Soc. Rev.* **44**, 47 (2015).

[19] O.P. Siwach, P. Sen, *Solid State Commun.* **148**, 221 (2008).

[20] V. Stanić, A.S. Radosavljević-Mihajlović, V. Živković-Radovanović, B. Nastasijević, M. Marinović-Cincović, J.P. Marković, M.D. Budimir, *Appl. Surf. Sci.* **337**, 72 (2015).

[21] T. Sakajiri, H. Yajima, T. Yamamura, *ISRN Biophysics* **2012**, 124803 (2012).

[22] M.J. Frisch, G.W. Trucks, H.B. Schlegel, G.E. Suzerain, M.A. Robb, J.R. Cheeseman Jr., J.A. Montgomery, T. Vreven, K.N. Kudin, J.C. Burant, J.M. Millam, S.S. Iyengar, J. Tomasi, V. Barone, B. Mennucci, M. Cossi, G. Scalmani, N. Rega, G.A. Petersson, H. Nakatsuji, M. Hada, M. Ehara, K. Toyota, R. Fukuda, J. Hasegawa, M. Ishida, T. Nakajima, Y. Honda, O. Kitao, H. Nakai, M. Klene, X. Li, J.E. Knox, H.P. Hratchian, J.B. Cross, V. Bakken, C. Adamo, J. Jaramillo, R. Gomperts, R.E. Stratmann, O. Yazyev, A.J. Austin, R. Cammi, C. Pomelli, J.W. Ochterski, P.Y. Ayala, K. Morokuma, G.A. Voth, P. Salvador, J.J. Dannenberg, V.G. Zakrzewski, S. Dapprich, A.D. Daniels, M.C. Strain, O. Farkas, D.K. Malick, A.D. Rabuck, K. Raghavachari, J.B. Foresman, J.V. Ortiz, Q. Cui, A.G. Baboul, S. Clifford, J. Cioslowski, B. Stefanov, G. Liu, A. Liashenko, P. Piskorz, I. Komaromi, R.L. Martin, D.J. Fox, T. Keith, M.A. Al-Laham, C.Y. Peng, A. Nanayakkara, M. Challacombe, P.M.W. Gill, B. Johnson, W. Chen, M.W. Wong, C. Gonzalez, J.A. Pople, Gaussian 09 (now Gaussian 16), Gaussian Inc., Wallingford (CT) 2016.

[23] S.F. Boys, F. Bernardi, *Mol. Phys.* **19**, 553 (1970).

[24] M. Sandstrom, G.W. Neilson, G. Johansson, T. Yamaguchi, *J. Phys. C Solid State Phys.* **18**, L1115 (1985).

[25] J.M. Hughes, M. Cameron, K.D. Crowley, *Am. Mineral.* **74**, 870 (1989).

[26] J.C. Elliott, *Structure and Chemistry of the Apatites and Other Calcium Orthophosphates*, Elsevier Sci. B.V., Netherlands 1994.

[27] N. Leroy, E. Bres, *Eur. Cell. Mater.* **2**, 36 (2001).

[28] H. Ishii, M. Ikeya, *Appl. Radiat. Isot.* **44**, 95 (1993).

[29] G.A. Waychunas, *Rev. Mineral. Geochem.* **48**, 701 (2002).

[30] D. Li, D. Jiang, J. Xie, *RSC Adv.* **5**, 12392 (2015).

[31] Z. Parang, A. Keshavarz, S. Farahi, S.M. Elahia, M. Ghoranneviss, S. Parhoodeh, *Sci. Iran. F* **19**, 943 (2012).

[32] B. Xia, L.N. Mandeng, N. Bondre, A. Dragan, C.D. Geddes, *Coll. Surf. A Physicochem. Eng. Asp.* **444**, 9 (2014).

[33] I. Lacatusu, N. Badea, A. Murariu, A. Meghea, *Nanoscale Res. Lett.* **6**, 73 (2011).

[34] B. Herzog, D. Hüglin, E. Borsos, A. Stehlin, H. Luthe, *Chimia* **58**, 554 (2004).

[35] K. Morabito, N.C. Shapley, K.G. Steeley, A. Tripathi, *Int. J. Cosmet. Sci.* **33**, 385 (2011).

[36] H. Althues, J. Henle, S. Kaskel, *Chem. Soc. Rev.* **36**, 1454 (2007).